Opportunities to Update the Model of Tank Closure Grout Aging (SRNL-STI-2012-00404) Based on Experimental Results by the Savannah River Ecology Laboratory

Miles E. Denham

November 2020

IEI

Inspection Experts, Inc.

This report was prepared by Panoramic Environmental Consulting, LLC under Professional Services Subcontract Agreement 2024 with Inspection Experts, Inc. and funded by U.S. Department of Energy – Office of Environmental Management

Disclaimer

Table of Contents

Table of Figures

Table of Tables

Executive Summary

The purpose of this report was to review the results of experiments on evolution of tank grout pore fluids performed by the Savannah River Ecology Laboratory (SREL) and reported in Seaman et al. (2020) and highlight opportunities for updating the model of tank grout degradation presented in Denham and Millings (2012). The SREL experimental results validate some assumptions used in the 2012 grout degradation model and provide information useful for updating the model. All experiments on tank grout degradation have limitations because of reaction rates and the enormous disparity between duration of the experiments and the duration of the degradation of the real tank grout system. Given these limitations, the experimental results form the basis for several recommendations for updating the grout degradation model:

1. It is recommended that calculation of a normative mineralogy for use in an updated model be based on the chemical analysis of the tank closure grout reported in Seaman et al. (2020).
2. It is recommended that the use of more recent C-S-H phase thermodynamic data be considered.
3. It is recommended that the mineral hemicarboaluminate be considered in any updated model.
4. It is recommended that uncertainty in hydration state be examined by running simulations of pore fluid evolution using normative mineralogies based on less than 100% hydration of cementitious materials.
5. It is recommended that consideration be given to the nature of Eh measurements versus modeled values and the possibility of using both in Performance Assessments.

Introduction

This report provides recommendations on updating the geochemical model used in Performance Assessments of the F-Area and H-Area Tank Farms (Denham and Millings, 2012) to simulate long-term leaching of radionuclides from the residual waste layer of high level radioactive waste tanks. The model developed in Denham and Millings (2012), hereafter referred to as the 2012 model, was based on the best thermodynamic and experimental data available at the time. Using the geochemical software, The Geochemist's Workbench®, the 2012 model calculated the reaction path of a normative mineralogy of the tank grout components leached with a fluid of an assumed composition. The resulting simulation produced curves of pH and Eh versus number of pore volumes of leachate flushed through a block of grout. These were then used to calculate solubilities of various radionuclides in the residual waste layer as pore fluid conditions evolve due to grout degradation. The Savannah River Ecology Laboratory has since done experiments simulating tank grout degradation (Seaman et al., 2020) using tank grout formulations and a leaching fluid of composition similar to the leaching fluid used in the 2012 model. The purpose of the experiments was to produce laboratory-scale data useful for updating the simulation of long-term chemical degradation and pore fluid evolution of tank grout in future Performance Assessments. This document compares the results reported in Seaman et al. (2020) to the 2012 model to assess opportunities to improve the simulation of long-term pore fluid evolution of tank grout.

This report was prepared by Panoramic Environmental Consulting, LLC under Professional Services Subcontract Agreement 2024 with Inspection Experts, Inc. (IEI). The contract held by IEI is funded by the US Department of Energy – Office of Environmental Management.

Summary of 2012 Model

One aspect of the F- and H-Area Tank Farm Performance Assessments is use of the results of a fate and transport model with limited geochemical capabilities to evaluate radiological dose from groundwater at locations downgradient of the tank farms. The waste tanks are being emptied of all liquid waste leaving a thin layer of residual solid radioactive waste at the tank bottoms. As part of closure, the emptied tanks are filled with tank closure grout to minimize future leaching of radionuclides and other contaminants from the residual waste layer. The fate and transport model simulates water infiltration through a protective cap over the tanks, passing through the tank closure grout, leaching radionuclides from the residual waste layer, and passing into groundwater. The fate and transport model predicts concentrations in groundwater of pertinent contaminants, leached from the residual waste layer, at various locations over thousands of years. Predicted annual dose from radionuclides is calculated from the predicted radionuclide concentrations for persons using groundwater or surface water from the designated locations over these long timeframes.

The 2012 model was constructed to enhance the geochemical capabilities by allowing the fate and transport model to consider leaching of radionuclides from the residual waste layer at chemical conditions that vary as tank grout degrades with time. The 2012 model made it possible to apply varying solubility controls on certain radionuclides as pore fluid composition in the residual waste layer evolves over thousands of years. The 2012 model was a reaction path model of grout degradation and not a reactive transport model. It calculated the evolution of pore fluid composition versus pore volumes of infiltrate passing through the tank grout. The fate and transport model then transformed the number of pore volumes to time, based on the simulation of water flow through the tank grout.
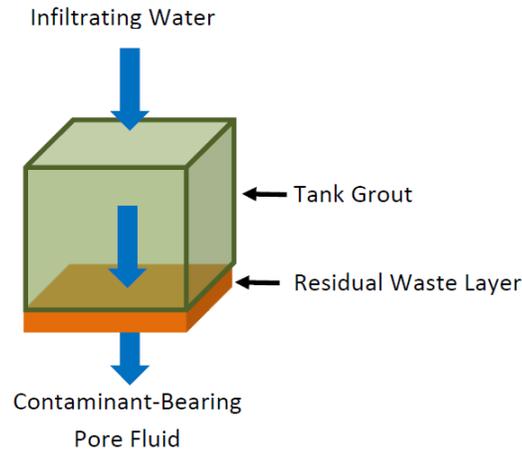
Figure 1: Simplified conceptual model of tank grout aging and pore fluid evolution.

The 2012 model was based on pore volumes of water flushing through a 1 cubic meter volume of tank grout with a fractional porosity of 0.21. A simplified conceptual model is shown in **Figure 1**. The minerals that make up the solid portion of the block were assigned based on a normative calculation that apportioned components of the total oxide composition of pre-hydrated grout to various post-hydration cementitious minerals. Appendix 1 contains a list of cementitious minerals and their chemical formulas referred to in this report. The first step of a reaction path model in The Geochemist's Workbench® is to recalculate the initial system so that minerals and fluid are in equilibrium, changing the mineralogy slightly from the normative calculation. These minerals are shown in **Table 1** together with all minerals allowed to react during the simulation. The prehydrated materials consisted of Ordinary Portland cement type I/II, blast furnace slag grade 100, class F fly ash, sand and gravel. The sand and gravel were assumed to be inert. Chemical reduction capacity was introduced to the grout block by assigning a mass of a reductant mineral that equaled the reduction capacity measured in blast furnace slag by Roberts and Kaplan (2009). Pyrite was chosen as the reductant mineral because of the known presence of iron sulfides in fly ash and reduced sulfur species in blast furnace slag. The choice of

Table 1: Minerals used in normative mineralogy calculation and other minerals allowed to react during simulation of grout degradation.

Normative Minerals	Initial Mineralogy Calculated by GWB[1]	Other Minerals Allowed in Simulation
Gibbsite	Gibbsite	Brucite
Gypsum	Tobermorite-D	C4AH13
Jennite-H	Jennite-H	$Fe(OH)_3$(amorphous)
Magnetite[2]	Magnetite[2]	Fe-Ettringite
OH-Hydrotalcite	Calcite	Jennite-D
SiO_2(amorphous)[2]	OH-Hydrotalcite	Maghemite
Pyrite[3]	Ettringite	Monocarboaluminate
	SiO_2(amorphous)[2]	Tobermorite-H
	Pyrite[3]	

1 – The Geochemist's Workbench®

2 – Not used in simulation

3 – Calculated based on measured reduction capacity

the reductant mineral determines the Eh of the pore fluids during early degradation of the grout, in addition accounting for reduction capacity.

The Geochemist's Workbench® Release 8 (Bethke and Yeakel, 2009) was used to run simulations of tank grout degradation. An equilibrium reaction path was calculated as infiltrate flushed through and reacted with grout minerals. The infiltrate composition was determined by equilibrating an average rainwater composition with kaolinite, allowing only amorphous silica to precipitate and fixing the fugacities of oxygen and carbon dioxide to those of atmospheric conditions. The infiltrate was flushed through the grout one pore volume at a time, with each pore volume completely displacing the previous one. Each pore volume of infiltrate was assumed to be isolated from the atmosphere and fugacities of oxygen and carbon dioxide in equilibrium with pore fluids were variable.

A hybrid thermodynamic database was created by adding cementitious minerals and their thermodynamic data from Lothenbach and Winnefeld (2006) and Kulik (2011) to the PHREEQC thermodynamic database (database "thermo_phreeqc" in The Geochemist's Workbench). Thermodynamic data for the iron minerals pyrite, magnetite, and maghemite were also updated.

The results of the simulation were curves of parameter values that are important to solubility of various radionuclides versus number of pore volumes of infiltrate reacted (**Figure 2**). The parameters important for calculating radionuclide solubilities are pH, Eh, and, for some radionuclides, the partial pressure of carbon dioxide. The parameters vary in step changes because of the nature of the model, delineating
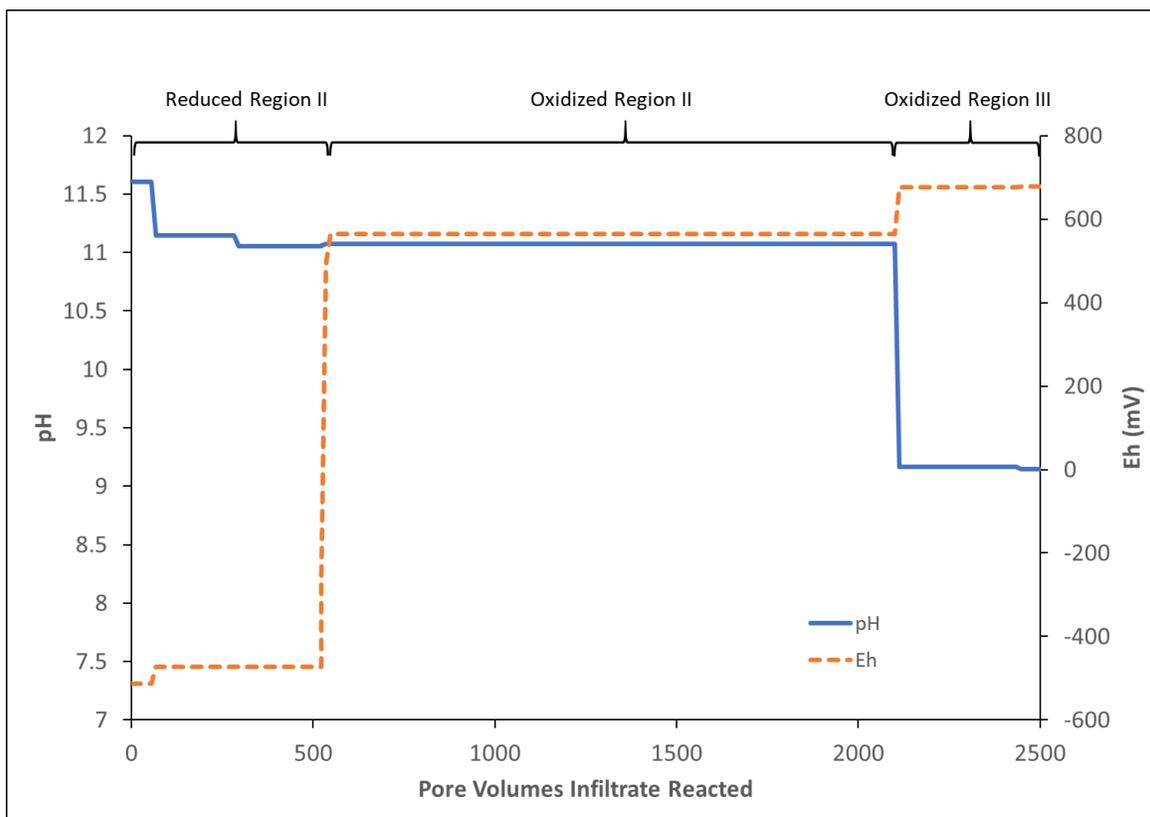

Figure 2: Chemical regions describing tank grout pore fluid evolution based on pH and Eh versus pore volumes of infiltrated fluid reacted curves produced by the 2012 model of grout degradation.

discrete chemical regions. These were named based on the model of pH evolution of cementitious pore fluids presented in Bradbury and Sarott (1995), with addition of a reducing region as shown in **Figure 2**.

In the Bradbury and Sarott (1995) model, Region I is characterized by a pH of approximately 13, elevated by the presence of dissolved sodium and potassium hydroxides. In the 2012 model, it was assumed that this initial pore fluid would rapidly flush from the system to avoid ionic strengths that were too high for accurate estimation of activity coefficients by Debye-Hückel-based models. Therefore, the simulation results begin at Region II.

Though there were sparse experimental data specific to Savanah River Site (SRS) tank closure grout performance prior to development of the 2012 model, it is important to note that the model is based on considerable experimental data from study of other cementitious systems. The chemical composition of the components that make up tank closure grout was known from Langton (2009). The chemical composition of the grout from which the normative mineralogy was calculated was based on the component compositions combined with the relative proportions of the components in tank closure grout from Stefanko and Langton (2011). The choice of cementitious phases to include in the original normative mineralogy, and the simulation as a whole, were based on studies of other cementitious systems (e.g., Hőglund, 2001; Lothenbach and Winnefeld, 2006). Thermodynamic data for the cementitious minerals comes from experimental studies that are incorporated into other cement modeling studies (e.g., Kulik, 2011; Lothenbach and Winnefeld, 2006). The choice of the mineral pyrite for imparting reducing capacity to the tank closure grout was based on identification of iron sulfides in smelting slags (e.g., Lottermoser, 2002). Finally, the amount of pyrite used in the initial mineralogy of the 2012 model was based on the measurement of the reduction capacity of granulated blast furnace slag by Roberts and Kaplan (2009).

Summary of Seaman et al. (2020) Experiments

Seaman et al. (2020) investigated evolution of tank grout pore fluids using batch leaching, enhanced leaching, and flow-through columns. The tank grout formulations used in the experiments contained cementitious materials at ratios that were the same or similar to those assumed in the 2012 model with one set containing blast furnace slag and one set without blast furnace slag. Sand was not added to added to the samples prior to hydration. Additional experiments done using controlled low-strength material (CLSM) are not discussed here because they are not relevant to the 2012 model. The tank grout samples were hydrated with laboratory tap water and cured for 90 days prior to the leaching experiments. Two different methods of curing were used. In one, the hydrated samples were wrapped in moist towels and placed in a laboratory cooler that was open to atmosphere. In the other, the samples were wrapped in moist towels and cured in an anoxic Coy Chamber atmosphere. The solution used to leach the grout samples was similar to the fluid assumed in the 2012 model, but at slightly higher pH (6 to 7 compared with 4.68) and lacking dissolved aluminum and silica. These differences, particularly absence of silica, may result in minor effects on pore water chemistry evolution.

Experiments were done using material that consisted of crushed grout pastes of two size fractions. The larger particle size had diameters between 0.5 and 2 mm (size-reduced) and the smaller size fraction had diameters less than 0.5 mm (crushed). The cured grout samples were size-reduced and crushed by hand using a rock hammer.

Batch experiments were done using 20 grams of sample (size-reduced or crushed) in 20 ml of leaching solution. The batch experiments were originally conducted under two different atmospheres, one open to air using the samples exposed to air during curing, the other in a Coy Chamber with a hydrogen/nitrogen atmosphere using the samples cured in the Coy Chamber. A third set of experiments was added conducted in a nitrogen atmosphere. The open and Coy Chamber cured samples were agitated and allowed to react with the leaching solution for 130 days. A set was then sacrificed for solids analysis. Another set was subjected to "enhanced leaching" for an additional 42 days by removing 10 ml of reacted fluid each day and replacing it with 10 ml of fresh solution. A third set was reacted with the initial 20 ml of solution for 172 days. To achieve an intermediate environment between oxic and extremely reducing, another group of samples was reacted with leaching solution for 141 days in a nitrogen atmosphere. Samples were regularly obtained for chemical analysis throughout the process.

Flow-through column studies were done using size-reduced material mixed with sand, as well as with intact monoliths made of the tank grout formulation hydrated with an amount of sand representative of grout used to fill waste tanks. The monoliths were packed with sand surrounding them in the columns. The influent leaching solutions were the same as those used in the batch studies. In one set of columns the influent solution was open to air. The other was closed and continuously purged with nitrogen. The flow rate of the influent solution was 5 ml/day. Eh and pH measurements were made on the column effluents.

Most of the column and batch experiments were terminated early because of restrictions in response to the COVID-19 pandemic. The batch experiments under a nitrogen atmosphere started later than others and were allowed to continue until their duration equaled other batch experiments.

The solids from the experiments were analyzed by x-ray fluorescence (XRF) for chemical composition and x-ray diffraction (XRD) for mineralogy. These analyses were done on the dry components that make up the tank grout samples, as well as leached and unleached tank grout samples.

Comparison of Experimental and Modeling Results

Comparison of the Seaman et al. (2020) experimental results to the 2012 model informs model improvement by allowing assessment of assumptions used to build the 2012 model, as well as the performance of the model versus measurements of pH and Eh. In the following discussion, assumptions that can be evaluated are presented as sub-sections with recommendations or important conclusions stated in italics for emphasis. Following the discussion of the 2012 model assumptions are sub-sections on comparison of modeled pH and Eh versus those measured in the experiments of Seaman et al. (2020).

Experiments by Walter and Dinwiddie (2019 and 2020) were like those performed by Seaman et al. (2020) and they will be referred to here as appropriate, though the focus of this report is on comparison of the Seaman et al. (2020) experimental results to the 2012 model. Walter and Dinwiddie (2019 and 2020) reacted pulverized SRS tank closure grout with a solution that mimicked the leachate in the 2012 model. Their batch experiments were in closed systems with no artificial atmosphere and were done primarily to assess the ability of tank closure grout to impose reducing conditions on pore fluids.

Assumption: Chemical composition of tank closure grout

The composite chemical analysis used in the 2012 model for the normative mineralogy calculation is compared to the measured chemical analysis from Seaman et al. (2020) in **Table 2**. The analyses are similar, yet differences in Al_2O_3, CaO, MgO, and SiO_2 are outside the range of analytical error. The only one of these that is likely to affect the modeled long-term performance of the grout is CaO. The higher CaO percentage measured by Seaman et al. (2020) would result in higher content of the hydrous calcium silicate phase (C-S-H) jennite-H in the normative mineralogy, and in turn, a slightly longer duration of Oxidized Region II. The differences in Al_2O_3 and MgO are unlikely to affect the modeled long-term performance of the grout because neither the mineral gibbsite $[Al(OH)_3]$ nor the mineral OH-hydrotalcite $[Mg_4Al_2(OH)_{14}\cdot3H_2O]$ are very reactive in the model. The difference in SiO_2 will not significantly affect the modeled performance of the grout because there is an excess of silica. *Nevertheless, it is recommended that calculation of a normative mineralogy for use in an updated model be based on the chemical analysis of the tank closure grout reported in Seaman et al. (2020).*

Table 2: Comparison of the chemical composition of dry mix of tank closure grout calculated for the 2012 model and the chemical analysis of tank closure grout samples by Seaman et al. (2020).

Component	2012 Model	Seaman et al. (2020)
Al_2O_3 (wt.%)	19.20	17.30
CaO	23.64	26.75
Fe_2O_3	5.02	5.73
K_2O	1.75	1.51
MgO	4.60	2.62
Na_2O	0.32	0.26
SO_3	1.15	1.46
SiO_2	44.31	41.20

Assumption: Cementitious mineralogy used to initiate 2012 model simulations

Characterization of the mineralogy of tank grout samples by Seaman et al. (2020) was done using x-ray diffraction (XRF), including extensive effort to quantify the mineral content of the grout. Comparison of the XRD results of real samples to the calculated mineralogy used to initiate the 2012 model suggests that the two are similar, but with some notable differences.

The XRD analyses indicate that most of the grout sample is amorphous (78.4 wt.%), as expected for cementitious samples. The C-S-H phases and other phases containing calcium, aluminum, and silica are poorly crystalline and have no distinct peaks identifiable by XRD. In the 2012 model the C-S-H phase was represented by the crystalline minerals jennite and tobermorite. Whether using crystalline minerals in place of poorly crystalline C-S-H results in a significant difference in model predictions of pH evolution is unclear. Yet, more recent thermodynamic databases incorporate poorly crystalline C-S-H phases and better representation of solid solution in the C-S-H phase (e.g., Giffaut et al, 2014; Prentice et al., 2018). *Hence, it is recommended that the use of more recent C-S-H phase thermodynamic data be considered.*

The non-C-S-H cementitious phases identified by Seaman et al. (2020) were hemicarboaluminate (4.07 wt.%), hydrotalcite (1.42 wt.%), ettringite (0.91 wt.%), kuzelite (0.78 wt.%), and portlandite (0.42 wt.%). A trace amount of strätlingite was also observed. Several phases that were likely present in the original

materials used to make the grout were also identified including mullite, quartz, hematite, magnetite, and calcite.

The main difference in mineralogy between that used in the 2012 model and that identified by Seaman et al. (2020) is the disposition of aluminum. All aluminum was divided between gibbsite and OH-hydrotalcite in the initial mineralogy of the 2012 model. The resulting equilibrium mineralogy that initiated the 2012 model included ettringite, using aluminum from gibbsite. Aluminum in the mineralogy observed by Seaman et al. (2020) is divided between amorphous phases, hemicarboaluminate, hydrotalcite, and ettringite. *It is recommended that hemicarboaluminate be considered in any updated model.* Regardless, the calculated mineralogy of the 2012 model is similar to the mineralogy observed by XRD analyses reported in Seaman et al. (2020).

Assumption: Extent of hydration of cementitious phases

An assumption in the calculation of a normative mineralogy for the 2012 model is that complete hydration of the cementitious phases will occur. The basis for this assumption was that leaching of the tank closure grout would begin only after the steel tank liner is breached by corrosion and water could pass through the grout. The tank closure grout would, thus, have decades to thousands of years to hydrate in 100% relative humidity, depending on the corrosion rate of the tank, prior to the beginning of leaching.

Experimental hydration studies of cements made with blast furnace slag and fly ash show that hydration is a slow process. Taylor et al. (2010) found that hydration continued after 14 months and was likely incomplete in a 20-year old sample. They also found that the nature of the C-S-H phase was significantly different between the 14-month and 20-year old samples. Prentice et al. (2018) showed that mineralogy changes as hydration continues.

The slow rate of cementitious material hydration is important because few experiments on cement aging span more than 2 years. The tank closure grout samples in the Seaman et al. (2020) experiments were hydrated for 90 days and the experiments lasted an additional 172 days. Thus, it is reasonable to assume that the samples were not completely hydrated. Nevertheless, it is also feasible that the tank grout does not hydrate completely within hundreds of years. *It is recommended that uncertainty in hydration state be examined by running simulations of pore fluid evolution using normative mineralogies based on less than 100% hydration of cementitious materials.* One way to this would be to remove the amount of aluminum and silica bound in the mullite and quartz of the Seaman et al. (2020) XRD analysis of tank closure grout and recalculate the normative mineralogy. Another way would be to assume different degrees of hydration of the tank closure grout components.

Assumption: Alkali metals are rapidly removed from the system

The pore fluids at the start of the 2012 model simulation of pore fluid evolution had much lower concentrations of alkali metals and a lower pH than occurs in freshly cured cement. High concentrations of alkali metals raise the ionic strength making calculation of activity coefficients less reliable. Hence, it was assumed that the alkali metals would flush out in the first pore volume of infiltration. The implied assumption is that there are no solid phases in the tank grout that release significant concentrations of alkali metals as they dissolve. This assumption is supported by the experimental results of Seaman et al. (2020). **Figure 3** (following page) shows the sodium and potassium concentrations in column experiments from Seaman et al. (2020). The concentrations are high at the start of the experiments and

decrease to very low concentrations early in the experiment, as the first 100 ml of effluent had been collected. Similar behavior is observed in the enhanced leaching batch experiments. This indicates that most of the mass of leachable alkali metals are in the initial pore water of the tank closure grout and will be flushed from the system by the first few pore volumes of infiltrate.
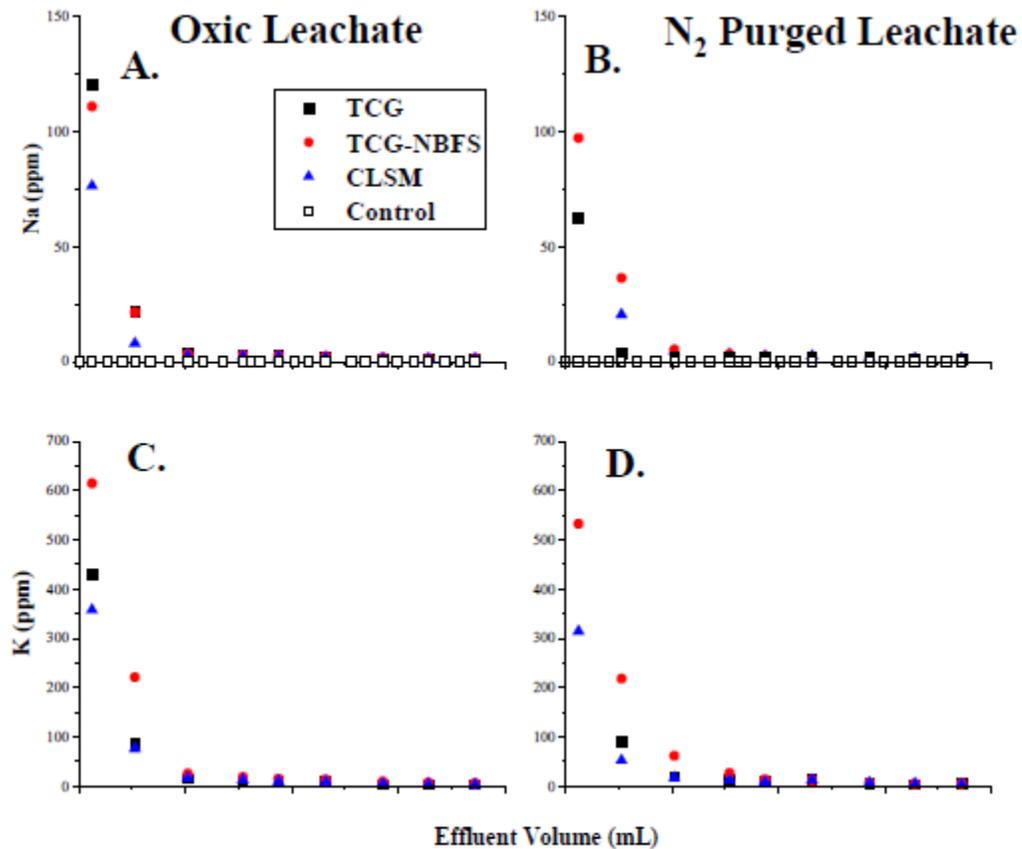
Figure 3: Alkali metal concentrations in effluent of column experiments of Seaman et al. (2020); each tick mark represents 100 ml of effluent.

Performance: pH Evolution

Comparison of pH evolution predicted by the 2012 model to the experiments of Seaman et al. (2020) is important because pH in tank closure grout pore fluids is critical to calculating radionuclide solubilities in water passing through the residual waste layer. In the 2012 model, the initial pH value was 11.6 and decreased to 11.1 in the first 67 pore volumes of infiltrate (**Figure 2,** page 4), where it remained for the duration of Reduced Region II and Oxidized Region II – across 2098 pore volumes. Evolution of pH in the batch experiments of Seaman et al. (2020) varies depending on the atmosphere in which the experiments were conducted (**Figure 4,** following page). Experiments open to air follow a pattern similar to the pH evolution predicted by the 2012 model. The initial pH is higher at 12.5, but pH decreases to

approximately 11.3 (11.1 for samples with no blast furnace slag) over the course of 150 days. The higher initial pH value reflects the presence of alkali metal hydroxides in solution, compared to the absence of alkali metals in the 2012 model. Values of pH evolve differently in experiments conducted under the two more reducing atmospheres. Under the nitrogen atmosphere, pH is initially approximately 12.1 and varies little over the course of the 150-day experiment. The initial pH under the Coy Chamber atmosphere is approximately 12.8, decreasing to 12.1 in the first 70 days and remaining relatively constant. Under all atmospheres the samples without blast furnace slag had pH values that were between about 0.3 to 0.6 pH units lower than samples with blast furnace slag.
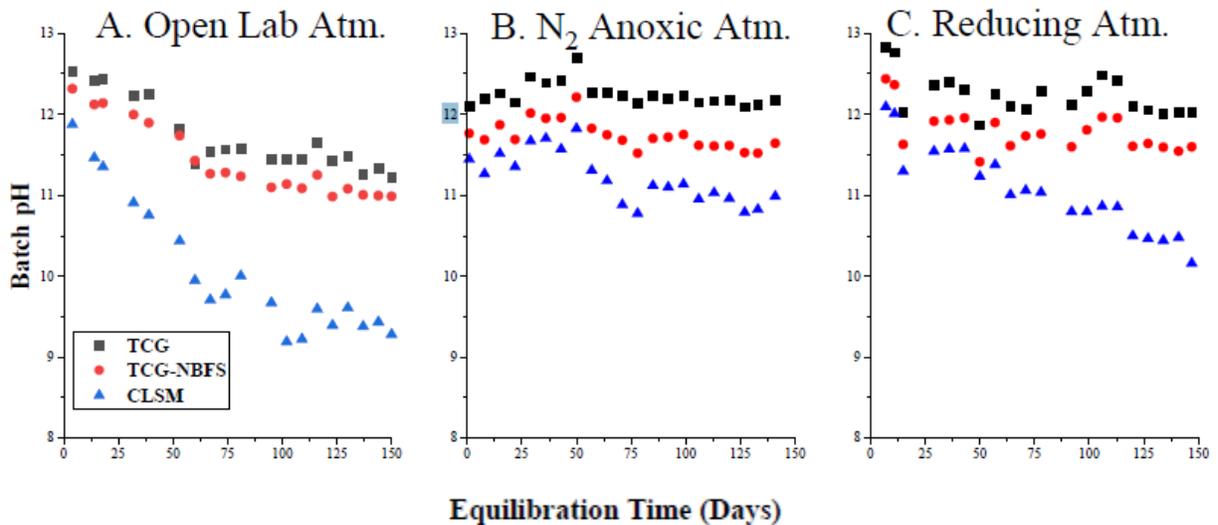
Figure 4: Evolution of pH during batch experiments reported in Seaman et al. (2020).

The final measured pH of the experiment exposed to air is similar to the calculated equilibrium pH throughout most of Region II in the 2012 model, yet this may be coincidental. The 2012 model is best represented by the Seaman et al. (2020) batch experiment done under a nitrogen atmosphere. The 2012 model assumes that the grout was not exposed to the atmosphere while reacting. Therefore, the only CO_2 and O_2 that could react was from dissolved gases in the infiltrate. The experiment by Seaman et al. (2020) that was open to the atmosphere allowed continual reaction with atmospheric CO_2. This resulted, as Seaman et al. (2020) note, in carbonation of C-S-H phases and precipitation of calcite. If carbonation of C-S-H was slower than dissolution of atmospheric CO_2, then the pH would have decreased by the reaction:

$$CO_{2(g)} + H_2O = CO_3^{-2} + 2H^+$$
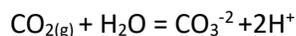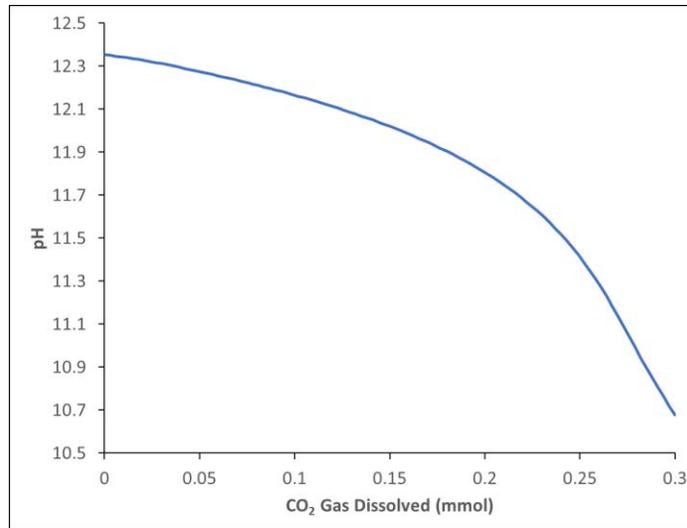
Figure 5: Effect of dissolving CO_2 gas on pH of cementitious pore fluids; calculated with The Geochemist's Workbench®.

Figure 5 shows the calculated effect of dissolving CO_2 gas in 20 grams of solution with an initial composition that is similar to the solution at the start of experiment open to the atmosphere. The initial pH is 12.35 and the calcium concentration is 37.5 ppm. As CO_2 dissolves, the pH decreases. This is likely the primary reaction driving decrease of pH in the experiment, rather than reaction with cementitious phases. This is supported by the absence of a significant pH decrease in the experiments with no CO_2 in their atmospheres. In the 2012 model the concentration of dissolved CO_2 is not high enough to significantly affect pH. The pH decrease in the model was driven by reaction with cementitious phases, as well as by the influx of dissolved silica. The silica in the model infiltrate was predominantly in the species H_4SiO_4, that produced acid by deprotonation to the species $H_3SiO_4^-$. There is further deprotonation in the model as $H_3SiO_4^-$ reacts with Ca^{+2} to form the aqueous complex $CaH_2SiO_4°$. Thus, silica in the modeled infiltrate does make some difference in the modeled pore fluid evolution.

The pH decreases in the column studies reported in Seaman et al. (2020) are more likely to represent actual reaction of cementitious materials. In these experiments, only the infiltrate was open to air or purged with nitrogen. CO_2 gas from the atmosphere could not continuously dissolve in pore fluids within the column contents. Hence, the pH curves are nearly identical for the two experiments (**Figure 6**, following page). The pH values are initially approximately 12.5 because of the presence of dissolved alkali metal hydroxides and decrease as these are flushed from the column. The final pH values, after >700 ml of effluent, approach those calculated for Region II in the 2012 model – pH=11.1.
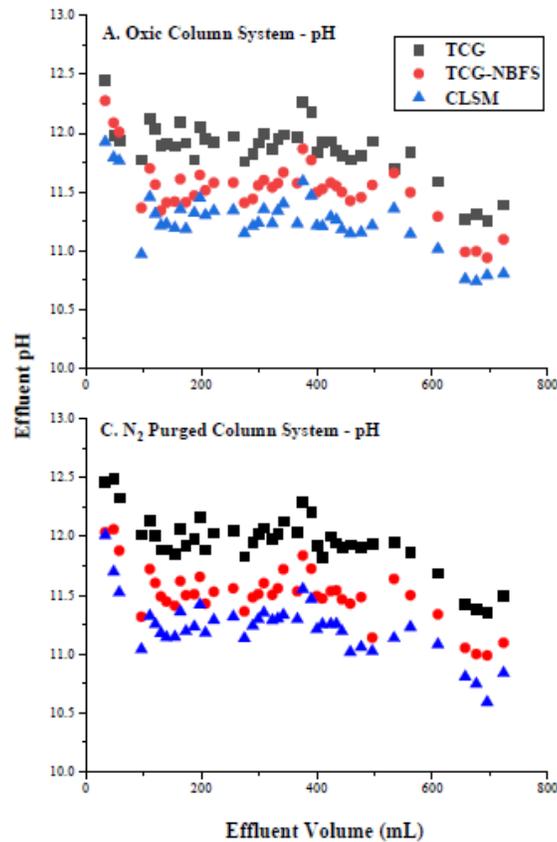
Figure 6: Effluent pH vs. effluent volume in column experiments of Seaman et al. (2020).

Performance: Eh Evolution

Redox potential, calculated in the 2012 model as Eh, is another "master" variable controlling solubilities of radionuclides subject to leaching from the residual waste layer in high level waste tanks. Dissolved oxygen was introduced into the tank closure grout by each pore volume of infiltration in the 2012 model. The Eh during Reduced Region II was calculated by the model to be -473 mV, in equilibrium with pyrite (**Figure 2,** page 4). When all pyrite was oxidized, the grout transitioned to Oxidizing Region II and Eh became controlled by equilibrium with dissolved oxygen at a value of 564 mV. When the transition to Oxidized Region III occurred, the pH decreased from 11.1 to 9.2, causing the Eh to increase to 676 mV. Natural hydrogeological systems rarely have Eh values that are in equilibrium with dissolved oxygen even when saturated with oxygen. Typically, they are more influenced by redox couples involving iron, manganese, nitrogen, and sulfur. Therefore, Denham and Millings (2012) described the Eh calculated by the 2012 model as an extreme case and recommended solubility values of radionuclides calculated at Eh values of +240 mV for Oxidized Region II and +290 mV for Oxidized Region III.

In the batch experiments reported in Seaman et al. (2020), Eh values were never as reducing as calculated in the 2012 model (**Figure 7,** following page). The lowest Eh in the experiment under a nitrogen atmosphere was approximately -120 mV, while the lowest Eh in the highly reducing

atmosphere of the Coy Chamber was -420 mV. Again, the experiments in the nitrogen atmosphere were the closest analogues to conditions assumed in the 2012 model. Eh values measured in the experiment open to the air were never below zero mV, the lowest being +120 mV. Eh values were generally lower in grout samples containing blast furnace slag in the experiments under a nitrogen atmosphere. This was not the case for experiments in the other two atmospheres, suggesting the atmospheres had more control on the Eh than reactions of the fluids with cementitious materials. This was noted in Seaman et al. (2020) for the Coy Chamber results. However, the Coy Chamber results present another interesting behavior: an increase in Eh with time. This was also the behavior in the experiments under nitrogen, but it can be argued that in these experiments the initial low Eh values were caused by reaction with small high surface area particles containing reduced iron or sulfur. Once these particles were oxidized the Eh increased. The highly reducing atmosphere of the Coy Chamber should have constrained Eh to highly reducing values if it was solely the atmosphere controlling the Eh.
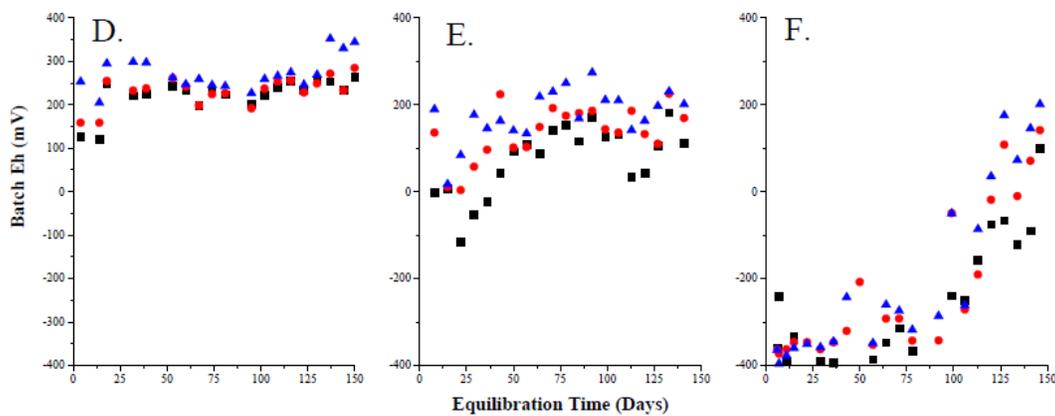

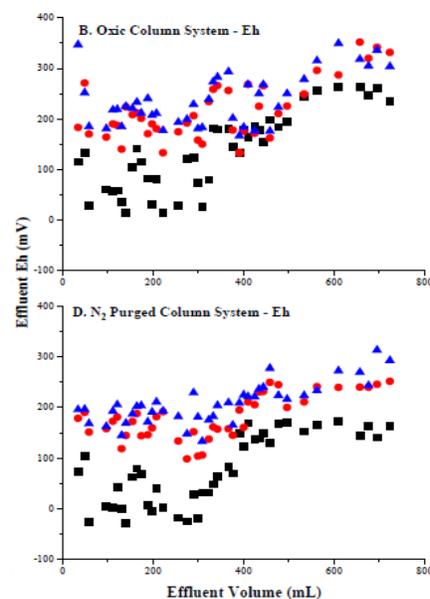Figure 7: Eh values (mV) vs. time in batch experiments of Seaman et al. (2020).

Figure 8: Eh vs. effluent volume in column studies of Seaman et al. (2020).

Eh values in the column experiments start near zero mV and increase with volume of effluent passed through the column (**Figure 8,** previous page). The atmosphere to which the infiltrate was exposed made little difference to the Eh values or their evolution and samples containing blast furnace slag had consistently lower Eh values than those without slag. These observations suggest that the Eh values in the column experiments were controlled by reaction with the cementitious materials.

It should be noted that the experiments of Walter and Dinwiddie (2020) achieved lower Eh values, reaching -300 mV in stirred tests with fresh pulverized tank closure grout samples. This may be due to the larger water to solid ratio, approximately 5:1 rather than 1:1 mass ratio, and the pulverization of samples in a jaw mill. If the pulverized samples contained a larger fraction of high surface area particles than the samples used by Seaman et al. (2020), then rates of reaction with cementitious materials would have been faster, allowing release of more reducing components. The larger water to solids ratio would allow a greater mass of cementitious material dissolution, increasing the probability of dissolving reducing components. Walter and Dinwiddie (2020) also measured sulfur species in the fluid after reaction. In addition to sulfate, they observed reduced sulfur species with relatively high concentrations of thiosulfate and minor sulfide and sulfite.

The Eh values of grout samples without slag are important for assessing the assumption of Denham and Millings (2012) that Eh values in Oxidizing Regions II and III are much lower than predicted by equilibrium with dissolved oxygen. In batch experiment with tank closure grout made without slag and open to the atmosphere, Seaman et al. (2020) measured a maximum Eh of +280 mV, consistent with the +240 and +290 mV assumed for Oxidized Regions II and III by Denham and Millings (2012). Walter and Dinwiddie (2020) measured Eh values between +200 and +300 mV for mixtures of Portland cement and fly ash.

It is recommended that consideration be given to the nature of Eh measurements versus modeled values and the possibility of using both in Performance Assessments. The 2012 model produces extremes at the oxidizing and reducing conditions. In the oxidizing regions, the 2012 model is constrained by equilibrium with dissolved oxygen. In the reducing region, Eh is controlled by selection of a mineral phase containing reduced species (e.g., pyrite). Measurement of Eh values in experiments of both Seaman et al. (2020) and Walter and Dinwiddie (2020) fall between these extremes. Yet, the meaning of measured Eh values is uncertain because of redox disequilibrium (Bethke, 2008). Thus, careful consideration must be given as to how Eh values are selected when calculating radionuclide solubilities. Appendix 2 discusses this in more detail.

Reaction Rates, Time, and Experimental Limits

Experiments on grout degradation are important for understanding the degradation process and parameterizing models of degradation. Yet, experimental results must be interpreted with the knowledge of their imitations. Experimental representation of the evolution of pore fluids in real grouted tanks is hindered by slow reaction rates and slow percolation of water through hydrated grout that cause evolution of the pore fluids to extend for long periods of time. Duration of experiments is on the order of months to years, whereas evolution of tank grout pore fluids is expected to occur over thousands of years (SRR, 2012). Grout will be hydrating at 100% relative humidity for a minimum of decades prior to regular exposure to infiltration. The contact time of infiltrating water with grout phases will be centuries to millennia. The minimum modeled travel time of water from the top of the tank grout

to the residual waste layer for the base case is 97 years, yet may be as long as 3000 years (Flach, personal communication). Thus, extrapolating the results of experiments to these timeframes is difficult.

Evolution of the grout pore fluids will result from three types of reactions. Hydration reactions of the grout components is the first phase of grout evolution. After water from outside a tank begins to infiltrate the grout, dissolution-precipitation reactions and oxidation-reduction reactions occur influencing evolution of pore fluids.

Use of partially hydrated cement samples in experiments will affect the chemical composition of fluids reacted with the samples. One result is that the Ca/Si ratio of the initial C-S-H phase will be different than in a more completely hydrated sample. Also, portlandite may be present in a less hydrated sample and absent in a more hydrated sample. Both of these will affect evolution of pH during leaching experiments. Furthermore, experiments conducted with partially hydrated slag cements may yield different Eh values and lower reduction capacity than experiments conducted with fully hydrated samples. This is because much of the reductant is contained in glassy phases of the slag and is not available until the slag is hydrated. Once the grout is fully hydrated, reduction capacity is available through slow dissolution of reduced sulfur and iron phases. It is uncertain whether experiments with relatively short contact times between fluid and grout achieve saturation with these phases and how the release of reductants compares to the real situation of extremely long contact times.

There is extensive literature on blended cement hydration and the following examples indicate that hydration takes months to years. Gruyaert et al. (2010) found unhydrated cement phases and slag in 50-50 blends after 28 months of hydration. Likewise, Vasconcelos et al. (2020) observed unhydrated clinker phases in the low pH (<11) Cebama reference cement after 18 months of hydration. Taylor et al. (2010) showed that hydration reactions continued for longer than a year in a blended cement sample by comparing C-S-H phase morphology and chemistry, as well as percent reacted slag, at 14 months and 20 years. Unreacted materials were still detected at 20 years. Berodier and Scrivener (2015) suggested that the decrease in pore size during hydration can slow the chemical reactions by limiting rate of diffusion of components into and out of pores. There have also been many studies showing hydration times of fly ash and slag activated by sodium hydroxide exceeds several months (e.g., Ben Haha et al., 2010; Ben Haha et al., 2011; Le Saoŭt et al.,2011).

Leaching of hydrated grout is dominated by dissolution-precipitation reactions including dissolution of alkali hydroxides, C-S-H, and carbonation of C-S-H. These reactions determine the pH of grout pore fluids. Reaction rates involving silicates are slower than those involving alkali hydroxides, yet may still be fast enough to approach equilibrium in long-term batch experiments. Reaction rates are proportional to particle surface area and, hence, fine-grained particles react faster than coarse-grained particles. If there is heterogeneity in mineralogy by particle size, then that can be reflected in batch leaching results. Seaman et al. (2020) attempted to control for this by crushing each sample so that all particles of a sample passed through a 2-mm sieve. Leaching experiments using fully hydrated (or as complete hydration as is possible) grout samples do provide useful information on the pH value of pore fluids. Obtaining useful information on the duration of a pH region is more difficult. The experiment must have enough replacement of leaching solution to dissolve and/or carbonate all C-S-H before useful information is obtained about how long Region II pH will last before transition to Region III. The Seaman et al. (2020) experiments did not achieve this because experiments were forced to terminate early.

Laboratory experiments attempting to replicate real oxidation-reduction conditions in grout face multiple difficulties. Rates of reaction of redox couples are typically slow and vary substantially. Thus, mineral-water systems at low temperature are typically not at redox equilibrium. Furthermore, Eh is complicated because certain couples, including sulfate-sulfide and dissolved oxygen-water, are not measured accurately by the platinum electrode normally used to measure Eh (Bethke, 2008). In grout systems, there is an additional issue of availability of reductant species. Each major component of the tank closure grout has some level of reducing capacity and blast furnace slag has the highest. It is thought that the reducing capacity is predominantly the result of reduced sulfur species in the glassy slag phases (e.g., Arai et al., 2017; Chaouche et al., 2017). For these to be available to poise the Eh at a reducing value, they must be released from the slag by hydration to another phase that slowly releases them to solution as it dissolves. The disparity between time-frames of experiments and evolution of real grout systems means it is difficult to extrapolate experimental results regarding Eh to the field. Short-term experiments may be further from redox equilibrium or be dominated by different redox couples than real systems. Nevertheless, real systems are unlikely to approach redox equilibrium as treated in the 2012 model. Additional discussion of Eh is presented in Appendix 2.

Conclusions

The experiments of Seaman et al. (2020) provide information that will be useful in updating high level waste tank grout aging models. X-ray diffraction analysis of grout samples observed phases that were not included in the 2012 model and should be. Additionally, pH values attained in the column studies are consistent with those calculated in the 2012 model and the assumption used in the 2012 model that alkali metals quickly flush out of the system was confirmed by the experiments. Eh values measured in the experiments were lower for slag containing grouts indicating that slag imparts reduce capacity. However, Eh values measured during early aging were not as low as calculated in the 2012 model. The model assumed redox equilibrium that results in very low Eh values in the Reducing Region and very high values in the Oxidizing Region. An important observation in the experiments of Seaman et al. (2020) is that the Eh values measured in grout containing no blast furnace slag are consistent with those selected by Denham and Millings (2012) for the oxidizing regions. The experiments provide no information on the duration of the grout degradation regions delineated in the 2012 model.

Recommendations for updating the model from comparison of the results of the Seaman et al. (2020) experiments to the 2012 model are:

1. It is recommended that calculation of a normative mineralogy for use in an updated model be based on the chemical analysis of the tank closure grout reported in Seaman et al. (2020).
2. It is recommended that the use of more recent C-S-H phase thermodynamic data be considered.
3. It is recommended that hemicarboaluminate be considered in any updated model.
4. It is recommended that uncertainty in hydration state be examined by running simulations of pore fluid evolution using normative mineralogies based on less than 100% hydration of cementitious materials.
5. It is recommended that consideration be given to the nature of Eh measurements versus modeled values and the possibility of using both in Performance Assessments.

Acknowledgements

References

Andersson, K., B. Allard, M. Bengtsson, and B. Magnusson, 1989. Chemical composition of cement pore solutions. *Cement and Concrete Research*, 19, 327-332.

Arail, Y., B.A. Powell, and D.I. Kaplan, 2017. Sulfur speciation in untreated and alkali treated ground-granulated blast furnace slag. *Science of the Total Environment*, 589, 117-121.

Ben Haha, M., G. Le Saoŭt, F. Winnefeld, B. Lothenbach, 2011. Influence of activator type on hydration kinetics, hydrate assemblage and microstructural development of alkali activated blast furnace slags. *Cement and Concrete Research*, 41, 301-310.

Ben Haha, M., K. De Weerdt, and B. Lothenbach, 2010. Quantification of the degree of reaction of fly ash. *Cement and Concrete Research*, 40, 1620-1629.

Berodier, E. and K. Scrivener, 2015. Evolution of pore structure in blended systems. *Cement and Concrete Research*, 73, 25-35.

Bethke, C.M., 2008. Geochemical and biogeochemical reaction modeling, 2nd Edition. Cambridge University Press, Cambridge UK.

Bethke, C.M.and S. Yeakel, 2009. The Geochemist's Workbench® (geochemical modeling software), Release 8.0 Reference Manual, University of Illinois.

Bradbury, M. H., Sarott, F., 1995. Sorption Database for the Cementitious Near-Field of a cement. *Cement and Concrete Research*, 36, 209-226.

Chaouche, M., X.X. Gao, M. Cyr, M. Cotte, and L. Frouin, 2017. On the origin of the blue/green color of blast-furnace slag-based materials: Sulfur K-edge XANES investigation. *Journal of the American Ceramics Society*, 2017, 1-10. DOI: 10.1111/jace.14670

Denham, M.E. and M.R. Millings, 2012. Evolution of chemical conditions and estimated solubility controls on radionuclides in the residual waste layer during post-closure aging of high level waste tanks. SRNL-STI-2012-00404, Savannah River National Laboratory, Aiken, SC.

Giffaut, E., M. Grivé, Ph. Blanc, Ph. Vieillard, E. Colàs, H. Gailhanou, S. Gaboreau, N. Marty, B. Madé, L. Duro, 2014. Andra thermodynamic database for performance assessment: ThermoChimie, *Applied Geochemistry*, 49, 225-236.

Gruyaert, E., N. Robeyst, N. De Belie, 2010. Study of the hydration of Portland cement blended with blast-furnace slag by calorimetry and thermogravimetry. *Journal of Thermal Analysis and Calorimetry*, 102(3), 941-951.

Höglund, L.O., 2001. Project SAFE: Modelling of long-term concrete degradation processes in the Swedish SFR repository. SKB Report R-01-08, Swedish Nuclear Fuel and Waste Management Co., Stockholm, Sweden.

Kempl, J. and O. Çopuroğlu, 2016. Eh-pH and main element analyses of Blast Furnace Slag Cement paste pore solutions activated with sodium monofluorophophate – Implications for carbonation and self-healing. *Cement and Concrete Research*, 71, 63-76.

Kulik, D.A., 2006. Improving the structural consistency of C-S-H solid solution thermodynamic models. *Cement and Concrete Research*, 41, 477-495.

Langton, C.A., 2007. Chemical Degradation Assessment of Cementitious Materials for the HLWTank Closure Project (U). WSRC-STI-2007-00607, Rev. 0. Washington Savannah River Company, Aiken, SC.

Langmuir, D., 1997. Aqueous Environmental Geochemistry. Prentice Hall, Upper Saddle River, NJ.

Le Saoŭt, G., M. Ben Haha, F. Winnefeld, and B. Lothenbach, 2011. Hydration degree of alkali-activated slags: A 29Si NMR study. *Journal of the American Ceramics Society*, 94, 4541-4547.

Lindberg, R.D. and D.D. Runnells, 1984. Ground water redox reactions: An analysis of equilibrium state applied to Eh measurements and geochemical modeling. *Science*, 225, 925-927.

Lothenbach, B. and F. Winnefeld, 2006. Thermodynamic modeling of the hydration of Portland cement. *Cement and Concrete Research*, 36, 209-226.

Lottermoser, B.,2002. Mobilization of heavy metals from historical smelting slag dumps, north Queensland, Australia. *Mineralogical Magazine*, 66(4), 475-490.

Painter, S.L. and R.T. Pabalan, 2009. Estimated longevity of reducing environments in grouted systems for radioactive waste disposal. Center for Nuclear Waste Regulatory Analyses, San Antonio, TX.

Prentice D.P., S.A. Bernal, M. Bankhead, M Hayes and J.L. Provis, 2018. Phase evolution of slag-rich cementitious grouts for immobilisation of nuclear wastes. *Advances in Cement Research* 30(8): 345–360, doi.org/10.1680/jadcr.17.00198

Roberts, K.A. and D.I. Kaplan, 2009. Reduction Capacity of Saltstone and Saltstone Components. SRNL-STI-2009-00637, Savannah River National Laboratory, Aiken, SC.

Seaman, J.C., S.P. Simner, and C. Logan, 2020. Aqueous and solid phase characterization of potential tank fill materials. SREL Doc.: R-21-0001, Savannah River Ecology Laboratory, The University of Georgia, Aiken, SC.

SRR, 2012. Performance Assessment for the H-Area Tank Farm at the Savannah River Site. SRR-CWDA-2010-00128, Revision 1. Savannah River Remediation LLC, Aiken, SC.

Stefanko, D.B. and C.A. Langton, 2011. Tanks 18 and 19-F Structural Flowable Grout Fill Material Evaluation and Recommendations. SRNL-STI-2011-00551, Savannah River National Laboratory, Aiken, SC.

Stumm, W. and J.J. Morgan, 1996. Aquatic chemistry: Chemical equilibria and rates in natural waters. John Wiley & Sons.

Taylor, R., I.G. Richardson, and R.M.D. Brydson, 2010. Composition and microstructure of 20-year-old ordinary Portland cement-ground granulated blast-furnace slag blends containing 0 to 100% slag. *Cement and Concrete Research*, 40, 971-983.

Vasconcelos, R.G.W., B. Walkley, S. Day, C.C. Tang, H. Paraskevoulakos, L.J. Gardner, C.L. Corkhill, 2020. 18-month hydration of a low-pH cement for geological disposal of radioactive waste: The Cebama reference cement, *Applied Geochemistry*, Journal Pre-Proof doi.org/10.1016/j.apgeochem.2020.104536.

Walter, G.R. and C.L. Dinwiddie, 2019. Tank Grout Water-Conditioning Tests – Status Report. Center for Nuclear Waste Regulatory Analyses, San Antonio, TX.

Walter, G.R. and C.L. Dinwiddie, 2020. Final Report: Tank Grout Water-Conditioning Tests – Fiscal Year 2019 Status Report. Center for Nuclear Waste Regulatory Analyses, San Antonio, TX. DOI: 10.13140/RG.2.2.24013.26080.

Appendix 1: Cementitious Minerals and Their Formulas

Mineral	Chemical Formula
Amorphous Silica	SiO_2
Brucite	$Mg(OH)_2$
C4AH13	$Ca_4Al_2O_7 \cdot 13H_2O$
Calcite	$CaCO_3$
Ettringite	$Ca_6Al_2(SO_4)_3(OH)_{12} \cdot 26H_2O$
Fe(OH)3(am)	$Fe(OH)_3$
Fe-Ettringite	$Ca_6Fe_2(SO_4)_3(OH)_{12} \cdot 26H_2O$
Gibbsite	$Al(OH)_3$
Gypsum	$CaSO_4 \cdot 2H_2O$
Hemicarboaluminate	$Ca_2Al(CO_3)_{0.25}(OH)_{6.5} \cdot 2H_2O$
Jennite-D	$Ca_{1.5}Si_{0.67}O_{2.84} \cdot 2.5H_2O$
Jennite-H	$Ca_{1.33}Si_{1.0}O_{3.33} \cdot 2.17H_2O$
Kuzelite	$Ca_2Al(SO_4)_{0.5}(OH)_6 \cdot 3H_2O$
Maghemite	Fe_2O_3
Magnetite	Fe_3O4
Monocarboaluminate	$Ca_4Al_2O_6(CO_3) \cdot 11H_2O$
Mullite	$3Al_2O_3 \cdot 2SiO_2$
OH-Hydrotalcite	$Mg_4Al_2(OH)_{14} \cdot 3H_2O$
Portlandite	$Ca(OH)_2$
Strätlingite	$Ca_2Al_2SiO_7 \cdot 8H_2O$
Tobermorite-D	$Ca_{0.88}Si_{0.67}O_{2.22} \cdot 1.83H_2O$
Tobermorite-H	$Ca_{0.66}Si_2O_{4.66} \cdot 1.5H_2O$

Appendix 2: The Eh Conundrum

Interpretation of Eh measurements in natural systems at near surface temperatures (for this discussion, 15-40˚C) have long been controversial and most agree that they are poor indicators or predictors of specific redox reactions (e.g., Lindberg and Runnells, 1984; Stumm and Morgan, 1996; Langmuir, 1997; Bethke, 2008). The reason is that natural aqueous systems have multiple redox couples involving common dissolved constituents such as oxygen, iron, manganese, and sulfur that are reacting at different rates. The measured Eh is some composite of the potentials of each of those reactions. Yet, matters are further complicated because some redox reactions seem to be catalyzed better by the platinum surface of an Eh electrode than others and the Eh measurement is biased toward those (Bethke, 2008).

This is a significant issue for modeling behavior of redox sensitive contaminants in Performance Assessments. The leachability of many important radionuclides, for example plutonium, neptunium, uranium, technetium, from waste is dependent on the redox state of the leaching fluids. The leachability of these depends on solubility and calculation of solubility requires an Eh value. The inclination of scientists and engineers is to value experimentally measured parameters over modeled parameters. But, what to do if the measured parameter is inherently flawed. This discussion cannot provide an answer. Rather, it reviews issues relating to Eh in tank closure grout now that measurements in grout-water systems have been made (Seaman et al., 2020; Walter and Dinwiddie, 2020), to inform decisions on modeling radionuclide leachability.

Eh is the potential of electrons in a system to promote oxidation or reduction reactions normalized to potential of the standard hydrogen electrode. It is related to Gibbs free energy of a redox reaction by the expression:

$$E = -\frac{G}{nF}$$

E is the electropotential of a reaction, G is the Gibb's free energy, n is the number of electrons transferred, and F is the Faraday constant. The Gibb's free energy expression can then be transformed to the Nernst equation in which Q is the ion activity product, just as in the Gibb's free energy expression.

$$\Delta E = \Delta E^0 - \frac{RT}{nF} \ln Q$$

If a chemical analysis of a water includes members of different redox couples, a Nernstian Eh can be calculated from the measured concentrations of the oxidized and reduced species of the various redox couples using the Nernst equation. This was done by Lindberg and Runnells (1984) for a number of analyses of natural waters. They found that the different redox couples were not in equilibrium with each other, the Nernstian Eh calculated for each couple was different. Equally as important, they found that the measured Eh was not the same as the Eh calculated from the redox couples. In most cases the measured Eh was closest to the calculated Eh for either nitrogen redox couples (nitrate, nitrite, ammonia) or the ferric/ferrous iron couple, but often far from those. In all cases, the measured Eh and the calculated Eh values for nitrogen, iron and sulfur couples were far from the calculated Eh of the oxygen couple. The disagreement between redox couples most likely reflects their different rates of reaction. The disagreement of the redox couples with Eh measurements reflects that fact that the

measurement is a composite of different redox couples with different reaction rates on the platinum electrode.

The work of Walter and Dinwiddie (2020) can be used to illustrate the difficulty with Eh measurements and redox couples. They measured Eh, pH, dissolved oxygen, and several sulfur species of different redox states in their experiments on leaching SRS tank closure grout. In an unstirred test, dissolved oxygen decreased to 7% saturation and measured Eh decreased to +175 mV. In a stirred experiment dissolved oxygen decreased to below detection and Eh decreased to -300 mV. **Table 3** shows the Nernstian Eh values calculated from measured concentrations of various sulfur species in the stirred experiment. The calculated Eh values for the unstirred test were similar though slightly higher. The calculated Eh values of the sulfur couples are lower than the measured Eh value. For the most part, the calculated values are similar to the calculated value of -470 mV in the 2012 model in which pyrite (FeS_2) was used to impart reducing capacity. The presence of thiosulfate ($S_2O_3^{-2}$), sulfide (S^{-2}), and elemental sulfur ($S_{(cr)}$) in fluids reacted with a slag containing grout are consistent with studies of sulfur speciation in solid blast furnace slag (Arail et al., 2017; Chaouche et al., 2017).

Table 3: Nernstian Eh calculated for sulfur redox couples from stirred experiment data in Walter and Dinwiddie (2020); $S_{(cr)}$ is crystalline elemental sulfur; measured Eh was -300 mV.

Redox Couple	Calculated Eh (mV)
$SO_4^{-2} - SO_3^{-2}$	-733
$SO_4^{-2} - S_2O_3^{-2}$	-597
$SO_4^{-2} - S_{(cr)}$	-591
$SO_4^{-2} - S^{-2}$	-543
$SO_3^{-2} - S_2O_3^{-2}$	-459
$SO_3^{-2} - S_{(cr)}$	-520
$SO_3^{-2} - S^{-2}$	-478
$S_2O_3^{-2} - S_{(cr)}$	-582
$S_2O_3^{-2} - S^{-2}$	-488
$S^{-2} - S_{(cr)}$	-407

The measured Eh value in the unstirred test, the calculated Eh based on measured dissolved oxygen saturation, and the calculated Eh at 100% dissolved oxygen saturation are shown in **Table 4**. The measured Eh is far lower than the calculated Eh from measured oxygen saturation and is between the Eh values calculated for sulfur couples and dissolved oxygen. The Eh value calculated at 100% oxygen saturation is shown for comparison because this was the assumption in the 2012 model for Oxidized Regions II and III.

Table 4: Comparison of measured Eh in unstirred experiment of Walter and Dinwiddie (2020) to calculated Eh based of 7% and 100% saturation with dissolved oxygen.

Measurement or Calculated Eh	Eh Value (mV)
Measured Eh	+175
Calculated Eh from 7% Oxygen Saturation	+519
Calculated Eh from 100% Oxygen Saturation	+537

Hence, the quandary in developing Eh values to be used to calculate radionuclide solubility is whether to use measured values or use values calculated in a model. If modeled values are to be used, then it is logical to use phases that contain reduced sulfur or reduced iron to impart reducing capacity because it is known that blast furnace slag and fly ash contain both. Yet, these will yield an Eh on the order of -400 to -500 mV, well below measured values. For the oxidizing regions, dissolved oxygen is the most realistic oxidant and will yield Eh values that are higher than measured Eh in oxidized grout.

The model could be made more consistent with measured Eh values by assuming the presence of redox couples in the infiltrate and the grout that give intermediate Eh values. However, manipulating a model without experimental evidence just to make it consistent with Eh measurements is difficult to justify given the uncertainty underlying Eh measurements. It would be more justifiable to simply use the measured Eh values to calculate radionuclide solubilities.

Denham and Millings (2012) used Eh values consistent with measurements in waters reacted with oxidized cements for Oxidized Regions II and III rather than using the Eh calculated by the 2012 model. The justification was that few Eh measurements in natural systems approach the Eh value in equilibrium with dissolved oxygen. Likewise, minerals containing reduced species such as Fe(II), Cr(III) and Mn(III), as well as organic matter, are commonly observed in aquifers that have been aerobic for hundreds of thousands of years. This suggests that the presence of dissolved oxygen does not necessarily dictate the redox state of some metals. In Denham and Milings (2012), radionuclide solubilities were calculated at the Eh values consistent with measurements in cement pore fluids as the base case and solubilities for key radionuclides calculated at the modeled Eh values were used as bounding cases. If this empirical approach is taken for the oxidized Eh values, it should also be taken for the reduced Eh values. This was not done in Denham and Millings (2012). Instead they presented curves of solubility versus Eh for key radionuclides to illustrate the effect on solubility if higher Eh values prevailed during Reducing Region II.

There are numerous published measurements of Eh in various cements that include those with and without blast furnace slag. Pabalan et al. (2009) have compiled several of these. Additional measurements are published in Andersson et al. (1989) and Kempl and Çopuroğlu (2016). Nevertheless, the Eh measurements of Seaman et al. (2020) and Walter and Dinwiddie (2020) are most pertinent because they were measured in water reacted with SRS tank closure grout. Seaman et al. (2020) report Eh measurements on tank closure grout with blast furnace slag that are pertinent to Reducing Region II and measurements on grout without slag that are pertinent to Oxidized Region II.

A grout degradation model is required to predict the duration of the reducing region, regardless of the approach taken to developing Eh values. By analogy to a battery, the Eh values are the voltage of the battery and the reduction capacity is the storage capacity of the battery. Reduction capacity is imparted to a model by choosing a phase that contains the reduced half of a redox couple. The logical phases for a grout containing blast furnace slag are ones containing either reduced iron or reduced sulfur or both. The concentration of the phase in the grout is determined from reducing capacity measurements of the grout and the reductive equivalents per gram of the reducing phase. The only other constraint is the solubility of the phase. If the phase is highly soluble, it will leach from the system in the first few pore volumes. Pyrite was chosen by Denham and Millings (2012), in part, because it is sparingly soluble in reduced systems and, thus, stoichiometrically reacts with dissolved oxygen. Another approach that may be closer to reality is to create a C-S-H like phase that contains reduced sulfur. The reduced sulfur from hydrated blast furnace slag is likely bound in an amorphous phase (Arail et al, 2017) with a relatively low

solubility. However, this approach would require careful consideration of the concentration of reduced sulfur, the solubility of the phase, and how these should be balanced to best represent transfer of reducing capacity from the grout solid phase to pore fluids.

The best approach to incorporate modeling and experimental results into radionuclide solubility controls during grout degradation is to use model results as bounding Eh values and experimental measurements of Eh as the base case. However, the experimental measurements used should be selected carefully to be sure they are as close to representative of real conditions as possible.